The use of vehicle acceleration measurements to estimate road roughness

A. GONZÁLEZ*†, E. J. OBRIEN†, Y.-Y. LI† AND K. CASHELL†

† School of Architecture, Civil Engineering & Landscape, University College Dublin, Ireland

*Corresponding author. Address: UCD School of Architecture, Landscape and Civil Engineering, Earlsfort Terrace, Dublin 2, Ireland. Phone: +353-1-7165512, Fax: +353-1-7167399, Email: arturo.gonzalez@ucd.ie

Abstract

Road roughness is a broad term that incorporates everything from potholes and cracks to the random deviations that exist in a profile. To build a roughness index, road irregularities need to be measured first. Existing methods of gauging the roughness are based either on visual inspections or using one of a limited number of instrumented vehicles that can take physical measurements of the road irregularities. This paper proposes the collection of data from accelerometers fixed in a specific vehicle type and the use of this data to estimate the road condition. While the estimate is approximate, accelerometers are being increasingly used by car manufacturers to improve suspension performance and the proposed method is relatively inexpensive to implement and provide road managers with constantly updated measurements of roughness. This approach is possible due to the relationship between the power spectral densities of road surface and vehicle accelerations via a transfer function. This paper shows how road profiles can be accurately classified using axle and body accelerations from a range of simulated vehicle-road dynamic scenarios.

Keywords: *Roughness; Classification; Dynamics; Accelerometer; ISO*

2000 Mathematics Subject Classifications: *34A30; 62M15*

1. Introduction

The analysis and maintenance of a road surface is a difficult problem that pavement engineers have been facing for many years. Detection of the condition of a road profile is important for many reasons, such as safety and economic savings, but profiling methods using direct measurements of the road itself are usually expensive [1-6]. The aim of this paper is to develop a method of estimating the general condition of a road by utilising technology that increasingly exists in everyday vehicles. It is becoming common in the luxury end of the car industry, that accelerometers are being fitted in the suspensions in order to improve suspension performance and increase ride comfort [7,8]. These accelerometers are effectively measuring the response of the vehicle to the road surface. It is proposed herein to collect and store these acceleration measurements to estimate the average road condition. Other researchers are developing methods for the collection of such data by road network management authorities [9]. The roughness estimate can be used to identify sections of road where the profile roughness has increased and hence to prioritise sections and optimise the use of profilometers for more detailed investigations.

Two popular methods to classify the roughness of a profile are the International Roughness Index (IRI) [10] and the International Standards Organisation (ISO) classification [11]. In this paper, the road condition is classified according to ISO, that uses Fourier analysis to calculate the Power Spectral Density (*PSD*) function of the surface. This *PSD* is compared to some boundaries that depend on the value of a geometric spatial mean, a, as described by equation (1).

$$PSD(\Omega) = \begin{cases} a(2\pi\Omega)^{-2} & \Omega \le 1/(2\pi) \\ a(2\pi\Omega)^{-1.5} & \Omega > 1/(2\pi) \end{cases} \qquad (1)$$

where Ω is spatial frequency in *cycles/m*. It classifies the profile into ‘A’ (very good), ‘B’ (good), ‘C’ (average), ‘D’ (poor) and ‘E’ (very poor) roughness indices as shown in figure 1 [11].

[Insert figure 1 about here]

2. Vehicle and road profile models

A 2-axle vehicle is modelled as a four degree-of-freedom suspension system. This model, known as a half-car, is illustrated in Figure 2.

[Insert figure 2 about here]

The sprung body mass of the vehicle, m_3, has vertical body displacement $y_3(t)$ and rotation $\varphi(t)$. The body mass moment of inertia is I_3. The two unsprung masses corresponding to the front and rear axles, m_1 and m_2, have vertical axle displacements $y_1(t)$ and $y_2(t)$ respectively.

The tyre stiffness is modelled as a linear spring of constant K_t and the suspension system as a linear spring K_s in parallel with a damper C_s. The horizontal distance from the centroid of the vehicle to the front axle is described as D_1, while the distance from the centroid to the rear axle is D_2 .The motion controlling the vehicle response when travelling at uniform speed is defined by the ordinary differential equations (2)-(4) [12]:

$$-I_3 \frac{d^2\varphi(t)}{dt^2} - D_1\left[Z_1(t) + Z_{b1}(t)\right] + D_2\left[Z_2(t) + Z_{b2}(t)\right] = 0 \tag{2}$$

$$-m_3 \frac{d^2 y_3(t)}{dt^2} - \left[Z_1(t) + Z_{b1}(t) + Z_2(t) + Z_{b2}(t)\right] = 0 \tag{3}$$

$$(m_i + m_{3i})g - m_i \frac{d^2 y_i(t)}{dt^2} + Z_i(t) + Z_{bi}(t) - R_i(t) = 0 \qquad i = 1,2 \tag{4}$$

where $Z_i(t)$ and $Z_{bi}(t)$ are the spring and damping forces between the i^{th} axle and the vehicle body respectively, m_i is the sprung mass corresponding to the i^{th} axle and $y_{3i}(t)$ is the displacement of the contact point between the i^{th} axle and the vehicle body.

$$Z_i(t) = K_s\left[y_{3i}(t) - y_i(t)\right] \qquad i = 1,2 \tag{5}$$

$$Z_{bi}(t) = C_s\left[\frac{dy_{3i}(t)}{dt} - \frac{dy_i(t)}{dt}\right] \qquad i = 1,2 \tag{6}$$

$$m_{31} = m_3 \frac{D_2}{D_1 + D_2} \tag{7}$$

$$m_{32} = m_3 \frac{D_1}{D_1 + D_2} \tag{8}$$

$$y_{3i}(t) = y_3(t) - (-1)^i D_i \varphi(t) \qquad i = 1,2 \tag{9}$$

The tyre force imparted to the road, $R_i(t)$, is given by equation (10).

$$R_i(t) = K_t\left[y_i(t) - r(x_i)\right] \geq 0 \qquad i = 1,2 \tag{10}$$

where $r(x_i)$ is the surface roughness corresponding to the location of the i^{th} axle at time *t*. This system of equations can be solved using the Runge-Kutta-Nyström method [13].

Based on the $PSD(\Omega_i)$ given by equation (1), the road surface irregularities can be generated using the discrete form of equation (11) [14].

$$r(x) = \sum_{i=1}^{N} \sqrt{2PSD(\Omega_i)\Delta\Omega}\cos(2\pi\Omega_i + \theta_i) \tag{11}$$

where x is the distance measured from the left end of the road, N, the total number of waves used to construct the road surface, $\Delta\Omega$, the frequency interval ($\Delta\Omega = (\Omega_{max} - \Omega_{min})/N$), and θ_i, the random phase angle uniformly distributed within $[0, 2\pi]$, that corresponds to the spatial frequency Ω_i, which is defined by equation (12):

$$\Omega_i = \Omega_{min} + (i - 0.5)\Delta\Omega \qquad i = 1, 2, 3...N \qquad (12)$$

3. Relationship between measured acceleration and road roughness

As result of unsprung mass motion being strongly influenced by the road profile, a measured time history of the vehicle accelerations, $\ddot{y}(t)$, can be used to describe the overall condition of the road profile, $r(x)$. Vibrations and road profile can be related in a linear system through a transform function defined by equation (13) [15,16].

$$H(\Omega) = PSD_{\text{acc}}(\Omega)/PSD_{\text{road}}(\Omega) \qquad (13)$$

where $PSD_{\text{acc}}(\Omega)$ and $PSD_{\text{road}}(\Omega)$ are the *PSD* for a frequency Ω due to the vehicle accelerations and road profile respectively. Once PSD_{road} is obtained, the road can be classified according to figure 1.

3.1 Calibration

In practice, these transform functions will be unknown, but they can be experimentally obtained using equation (13) and driving the vehicle over a measured profile. Once the transform function is calibrated, it can be used to classify any other profile, although periodic calibrations of $H(\Omega)$ are recommended. For the purpose of illustrating this procedure, a theoretical known road profile is generated. Then, a 'typical' 2-axle vehicle is excited with this profile using equations (2)-(10). Finally, the transform function of the vehicle is obtained from the *PSD*'s of road profile and simulated vehicle accelerations via equation (13). All calculations are carried out using MATLAB software [17,18].

Figure 3 shows the generated random road profile, classified by ISO as 'D' (poor). It is made up of 8001 spatial frequencies between 0.01 *cycles/m* and 4 *cycles/m*.

[Insert figure 3 about here]

Table 1 shows the values used for the parameters of the 'typical' half-car model employed in the simulation [16,19].

[Insert table 1 about here]

Axle and body mass accelerations, $\ddot{y}_1(t)$, $\ddot{y}_2(t)$ and $\ddot{y}_3(t)$, are illustrated in the figures 4(a), (b) and (c) respectively for a speed of 50 *km/h*.

[Insert figure 4 about here]

Then, the *PSD* of axle accelerations are calculated. However, because FFT uses a constant bandwidth, it over-exaggerates the fluctuations at high frequencies. This problem is overcome applying a smoothing procedure defined in [11]. The resulting smoothed *PSD* is illustrated in log-log scale in figure 5 for the road profile and in figure 6 for vehicle accelerations.

[Insert figure 5 about here]

[Insert figure 6 about here]

Figure 7 shows the calibrated transform functions for each vertical acceleration variable in this half-car model, derived from applying equation (13) to the figures 5 and 6.

[Insert figure 7 about here]

This function can be used to transform the *PSD* for axle or body accelerations to the *PSD* for the road profile and vice versa. For unknown road profiles, it can be used to find the *PSD* of the profile from axle or body acceleration measurements.

4. Numerical testing

4.1 Validation for different road profiles

Two new theoretical profiles are generated with the same spatial frequency range (0.01 *cycles/m* ~ 4 *cycles/m*) but different geometric spatial means, falling into classes 'C' and 'D'. The axle and body accelerations due to the crossing of the 'typical' half-car model (as defined in table 1) are obtained for a speed of 50 *km/h*. The *PSD* of the road profile is estimated from the *PSD* of axle and body accelerations using the transform functions of figures 7(a) and 7(b) respectively. Figures 8 and 9 compare the 'true' *PSD*, directly obtained from the road profile, to the estimated *PSD* for both road profiles when using front and rear axle accelerations respectively. It can be seen that both axle acceleration measurements can be used for an estimate of the *PSD* and accurately classify the road without the need for profiling equipment. A small deviation appears between 0.07 and 0.08 cycles/m (about 1 Hz, close to the body modes of vibration) of the PSDs in these two figures.

[Insert figure 8 about here]

[Insert figure 9 about here]

Figure 10 does the same comparison when using body accelerations. Sprung mass accelerations seem to provide a road spectra as accurate as the unsprung masses, except for small deviations at high frequencies and a significant peak around 0.5 cycles/m, about 7 Hz, related to axle hop interference. The road class can be reasonably predicted once the spectra is not falling very close to the divisory line between two road classes.

[Insert figure 10 about here]

4.2 Validation for different speeds

When measuring axle accelerations, the vehicle may drive at different speeds depending on traffic conditions. It is therefore important to evaluate the sensitivity of the transform function to speed. Figure 11 shows the 'true' and estimated *PSD* when driving the same vehicle at different speeds if using one only transform function (corresponding to 50 *km/h*). It is found that the closer the driving speed to the calibration speed, the more accurate the results become.

[Insert figure 11 about here]

Hence, accuracy can be improved by using a set of transform functions for a range of speeds and choosing that transform function appropriate to the speed closest to that for which axle accelerations are taken. Transform functions are illustrated in figure 12 for 40, 45, 50, 55 and 60 *km/h* speeds.

[Insert figure 12 about here]

Calibration of the transform function every 5 *km/h* is found to provide sufficient accuracy for a correct ISO classification. For example, *PSD* results of figure 10 are obtained using a transform function calibrated at 40 *km/h* for axle measurements taken at 42 *km/h*.

[Insert figure 13 about here]

4.3 Validation for a vehicle fleet

The *PSD* of front axle accelerations in the temporal frequency domain (*cycles/s*), *PSD*(*f*), can be obtained by dividing the *PSD* of axle accelerations in the spatial frequency domain, *PSD*(Ω) (figure 6(a)), by speed and the result is illustrated in figure 14.

[Insert figure 14 about here]

It can be seen that the critical frequency, where the peak values of *PSD*(*f*) occur, is 10.56 *cycles/s*, which represents axle hop frequency. It can be assumed that the *PSD* due to axle acceleration measurements will be similar if the axle hop natural frequency is similar and

other parameters vary within a reasonable range. In other words, if the transform function calculated for a particular vehicle was applied to the axle accelerations from other vehicles with similar properties, a reasonable degree of accuracy can be expected.

In order to test this assumption, the accelerations of six vehicles of the same type (eg., a fleet of public service vehicles) are simulated using the parameters specified in table 2.

[Insert table 2 about here]

Only the transform functions of the 'typical' half-car or calibration vehicle (figure 9) are employed to determine the *PSD* of the road profile from the axle accelerations of each vehicle. Figure 15 shows the *PSD* results for each of the six scenarios. It is found that the closer the axle hop frequency of the test vehicle is to the calibration vehicle, the more accurate the estimate. It can be concluded that the transform function of the calibrated vehicle can be used to estimate road roughness accurately once the vehicle has similar axle hop frequency and vehicle parameters.

[Insert figure 15 about here]

4.4 Validation for noise-corrupted acceleration data

The results discussed so far has been somewhat idealised because they have ignored the effects of noise. For high-quality sensors, the average power of the measurement noise will be small in comparison to the average power of the underlying accelerations. However, the noise power is typically spread out over a range of frequencies, and therein lies the problem. An additive noise model is used here to describe the noisy data that invariably is part of the measurements. So, the simulated acceleration, $a(t)$, is calculated as the sum of the true acceleration, $\ddot{y}(t)$, and the noise, $n(t)$:

$$a(t) = \ddot{y}(t) + n(t) \qquad \text{for any instant } t \tag{14}$$

The noise, $n(t)$ is zero-mean and described by its variance σ_n^2. The impact of the noise on the signal is described by the Signal to Noise ratio (*S/N*), which is given by:

$$S/N = \frac{\sigma_y}{\sigma_n} = \sqrt{\frac{\sigma_a^2}{\sigma_n^2} - 1} \tag{15}$$

where σ_y^2 and σ_a^2 are the variances of the true and the recorded accelerations respectively.

The algorithm is tested for the accelerations of the front axle shown in figure 4(a), which are corrupted with different levels of noise. Following smoothing procedure described in section 3.1, figure 16 shows the original and smoothed (*PSD*s of the noise-free ($\ddot{y}(t)$) and noise-corrupted accelerations ($a(t)$) for *S/N* of 20 (relative error in measurement of 5%), 10

(relative error of 10%) and 5 (relative error of 20%). It can be seen how the influence of noise on the PSD is very relevant for low frequencies, but it hardly has any effect on the high frequencies, even for low S/N.

[Insert figure 16 about here]

One hundred different noise signals ($n(t)$) are randomly generated varying the initial seed for each of the three S/N, which results into a total of 300 noise-corrupted acceleration samples being tested. The 100 estimated PSD's of road profiles are shown and compared to the 'true' PSD for each S/N in figure 17. If taking into count only the low frequency components, the deviations introduced by noise classify the road into a poorer class than in reality. The higher *S/N*, the poorer prediction for the low frequencies class. For the simulations under study, *S/N* of 20 will accurately classify the road class as 'D' except for very low spatial frequencies (figure 17(a)). *S/N* of 10 will classify the road class as 'E' for spatial frequencies below 0.04 cycles/m (figure 17(b)), while *S/N* of 5 will classify the road as 'F' for spatial frequencies below 0.04 cycles and as 'E' for spatial frequencies between 0.04 and 0.1 cycles/m (figure 17(c)). However, the influence of *S/N* on the high spatial frequency components of the spectra is not so important, and once frequencies are above 0.1 cycles/m, the road class is generally accurately predicted regardless the noise level.

[Insert figure 17 about here]

5. Conclusions

Current methods of estimating the road condition generally involve taking direct measurements of the profile using lasers or other measuring devices. Although there have been major improvements in recent years in the quality of road profiling equipment, these devices remain expensive to purchase, inefficient in terms of time and specialized in terms of operation. With maintenance and construction costs demanding a large portion of road management authorities budgets, this paper has presented a convenient, fast and economical method of estimating the road condition, using data harnessed from vehicle accelerometers. Then, the *PSD* of a road profile can be estimated from the *PSD* of the axle or body accelerations measured over the road profile. Such an approach requires prior knowledge of the vehicle transform function. This transform function depends only on vehicle parameters and it can be obtained by dividing the *PSD* of accelerations measured over a known profile by the *PSD* of that profile.

Computer simulations of half-car models have been carried out to analyse the sensitivity of the proposed road classification method to road roughness, speed, vehicle parameters and noise. Although it is hard to predict the exact interaction between a vehicle and a road in a simulation and the vehicles that are used are somewhat simplified, the findings give definite indications of the good levels of accuracy for the *PSD* estimate. The method is shown to be robust enough for a number of road profiles, vehicle speeds and dynamic scenarios. The possibility of using a fleet of vehicles to calculate profiles simultaneously is also

successfully tested. This would be far more time-efficient than using a single vehicle and opens up the possibility of using data from existing public sector vehicle fleets. In the presence of a significant random noise component, the low spatial frequency components of the road are classified into unrealistic poorer classes, but high spatial frequency components are generally classified within the correct road class. It has been shown how data from accelerometers fixed to the sprung mass can give a road spectra as accurate as axle acceleration data. Nevertheless, axle accelerations seem to provide slightly better estimates of the *PSD* than body accelerations for high spatial frequencies, which have been shown to be less sensitive to noise. Once the *PSD* of the road is identified, it is possible to generally classify the road as being very good/good/poor etc., thereby prioritising the roads that need further attention. Should a particular road be classified as poor for example, a more detailed investigation of the profile could then be carried out using specialised equipment such as profilometers.

Acknowledgements

The authors wish to acknowledge the financial support provided by the Irish Research Council for Science, Engineering and Technology (IRCSET) *Embark Initiative*.

References

[1] Hveem, F.N., 1960, Devices for Recording and Evaluating Pavement Roughness, Highway Research Board Bulletin, 264, 1-26.

[2] Perera, R.W. and Kohn, S.D., 2002, Issues in Pavement Smoothness: A summary Report, National Cooperative Highway Research Program, Transportation Research Board, National Research Council, March.

[3] Hu, F.X., 2004, Development Of A Direct Type Road Roughness Evaluation System, Master Thesis, Department of Civil and Environmental Engineering, College of Engineering, University of South Florida.

[4] Fawcett, G.A., Bennett, C.R. and Ollerenshaw, D.G., 2002, Flexible Low-Cost Data Capture Technology for Road Networks, MWH New Zealand Ltd.

[5] Spangler, E.B. and Kelley, W.J., 1964, GMR Road Profilometer. A method for Measuring Road Profile, Research Publication GMR-452, General Motor Research Laboratory, Warren Michigan, 44.

[6] Sayers, M.W. and Karamihas, S.M., 1996, Interpretation of Road Roughness Profile Data-Final Report, Federal Highway Administration, 25-26.

[7] Macdonald, G.A., 1990, Accelerometers for vehicle chassis systems, IEE colloquium on Chassis Electronics, Sensors & Microelectronics Dept., Lucas Automotive Ltd., Sohihull.

[8] Aburya, T., Kawanishi, M. and Hamada, T., 1990, Development of an electronic control system for active suspension, Proceedings of the 29th Conference on Decision and Control, IEEEE, Hawaii.

[9] 'INTRO' - cooperative systems for intelligent roads, a European sustainable surface transport research project, 2006, Available online at http://ec.europa.eu/research/transport/news/article_3396_en.html (accessed 15 May 2006).

[10] Sayers, M.W., Gillespie, T.D. and Paterson, W.D.O., 1986, Guidelines for Conducting and Calibrating Road Roughness Measurements, World Bank Technical Paper Number 46.

[11] ISO 8608:1995, 1995, Mechanical Vibration-Road Surface Profiles-Reporting of Measured Data, International Standards Organisation.

[12] Frýba, L., 1972, *Vibration of Solids and Structures under Moving Loads* (Noordhoff, Groningen, Netherlands).

[13] Kreyszig, E., 1983, *Advanced Engineering Mathematics* (John Wiley & Sons Inc, New York).

[14] Silva, J.G.S., 2004, Dynamical performance of highway bridge decks with irregular pavement surface, *Computers & Structures*, **82**, 871-881.

[15] Cebon, D., 1999, *Handbook of Vehicle-Road Interaction* (Swets & Zeitlinger).

[16] Wong, J.Y., 1993, *Theory of Road Vehicles* (John Wiley and Sons).

[17] Ifeachor, C.I. and Jervis, B.W., 1993, *Digital Signal Processing, A Practical Approach* (Addison-Wesley Publishers Ltd.).

[18] Schilling, R.J. and Harris, S.L., 2000, *Applied Numerical Methods for Engineers Using MATLAB and C* (Brooks/Cole Publishing Company).

[19] Sayers, M.W. and Karamihas, S.M., 1998, The Little Book of Profiling, University of Michigan.

List of figures

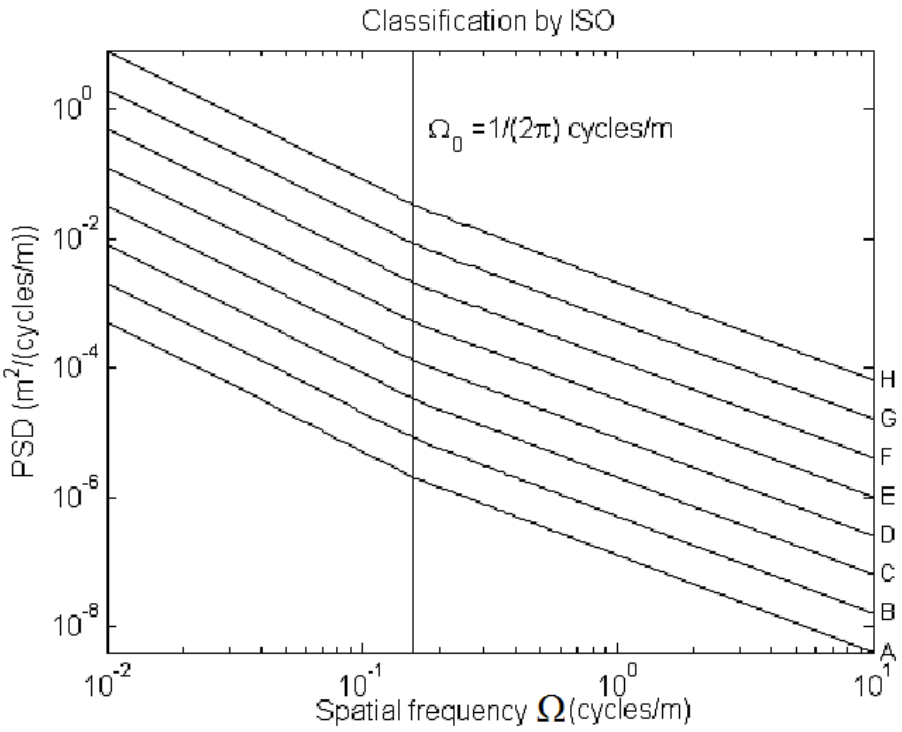

Figure 1. Classification of road roughness by ISO

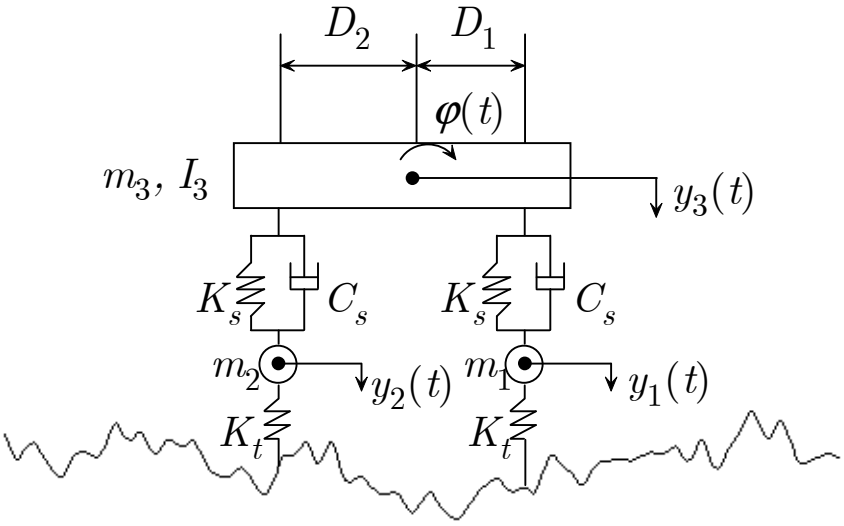

Figure 2. Half-car model

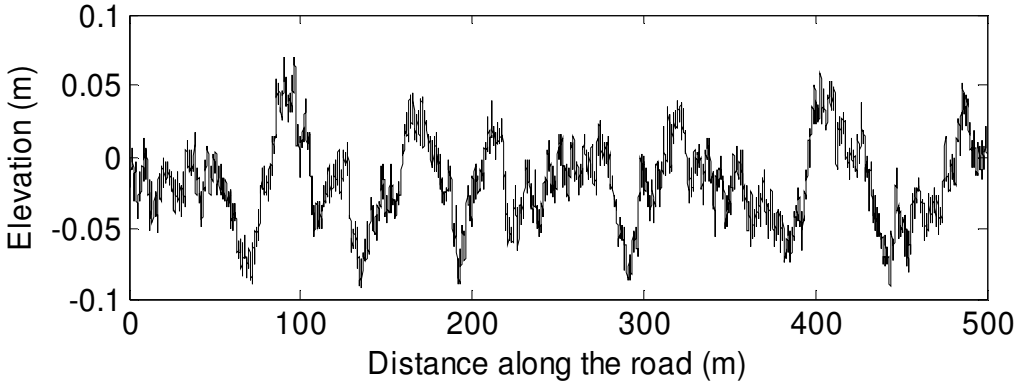

Figure 3. Class ‘D’ road profile

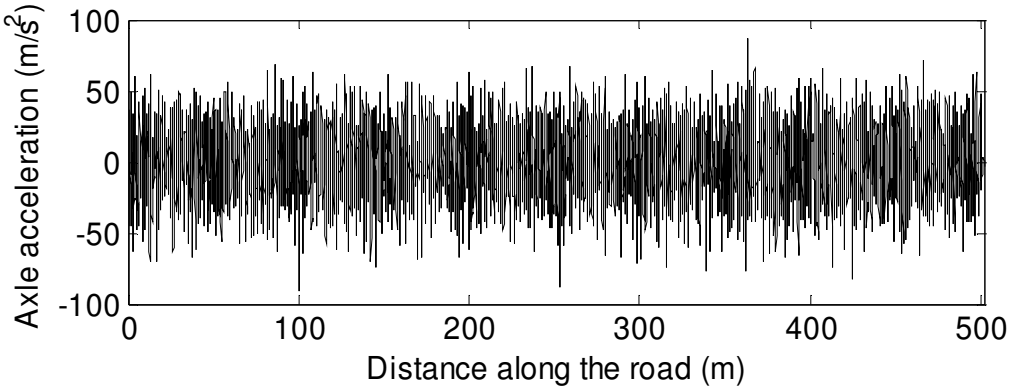

(a)

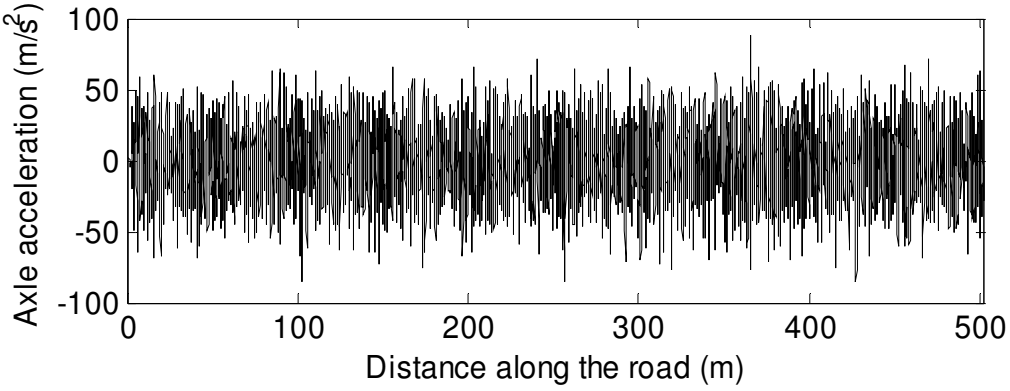

(b)

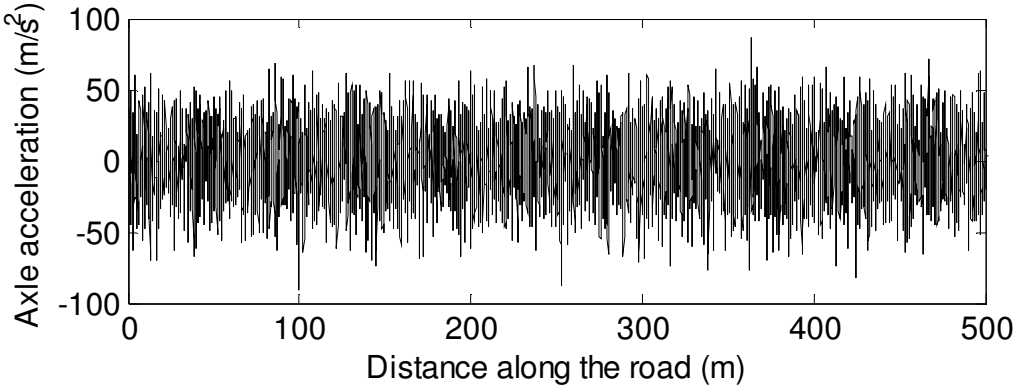

(c)

Figure 4. Vehicle accelerations: (a) Front axle $\ddot{y}_1(t)$, (b) Rear axle $\ddot{y}_2(t)$, (c) Body $\ddot{y}_3(t)$

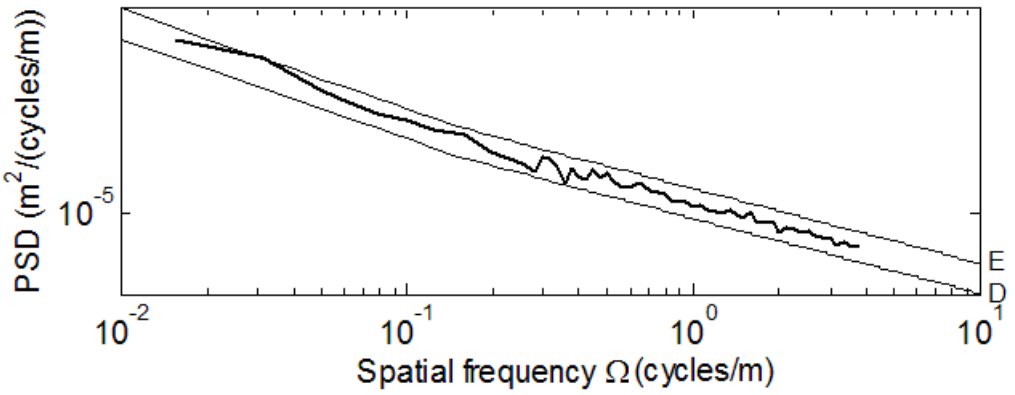

Figure 5. Smoothed *PSD*(Ω) of the road profile

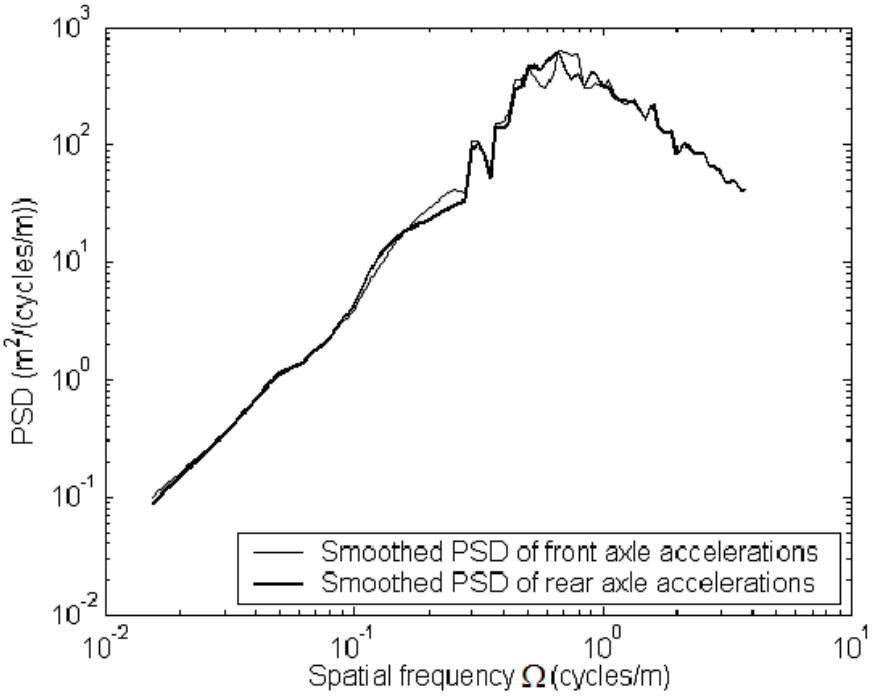

(a)

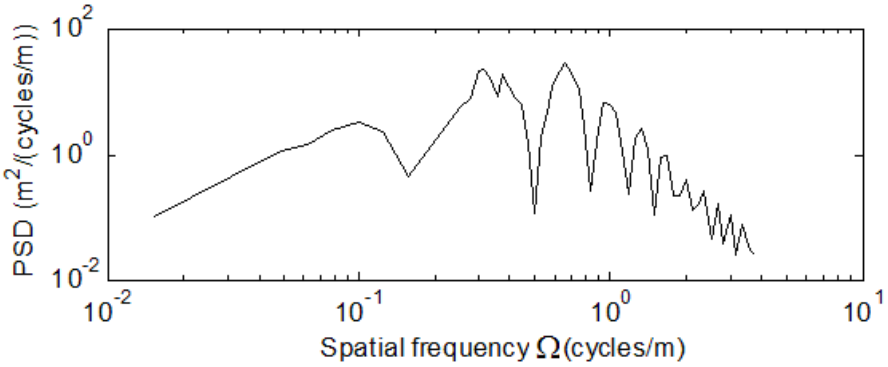

(b)

Figure 6. Smoothed *PSD*(Ω) for: (a) Front and rear axle accelerations, (b) Body accelerations

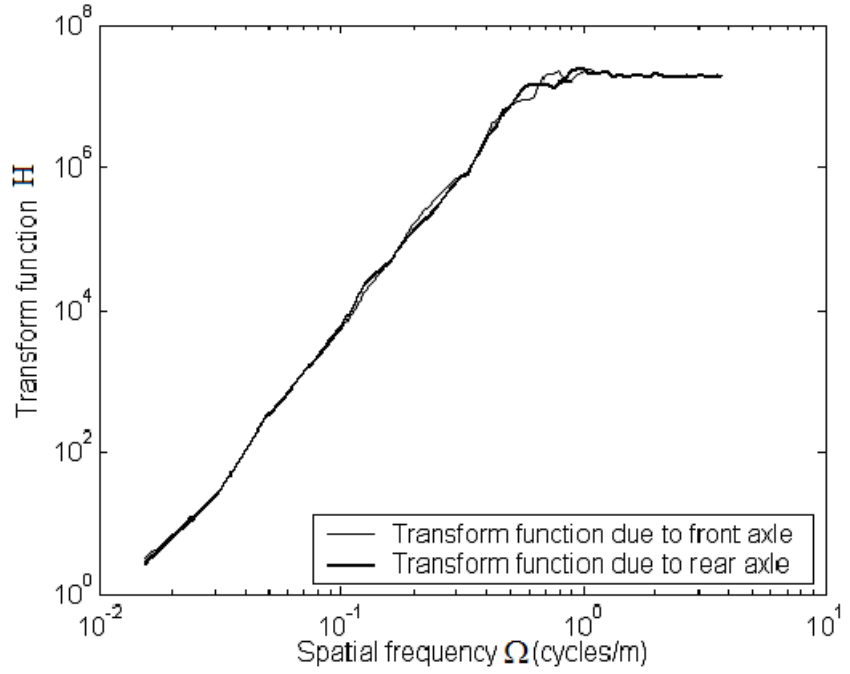

(a)

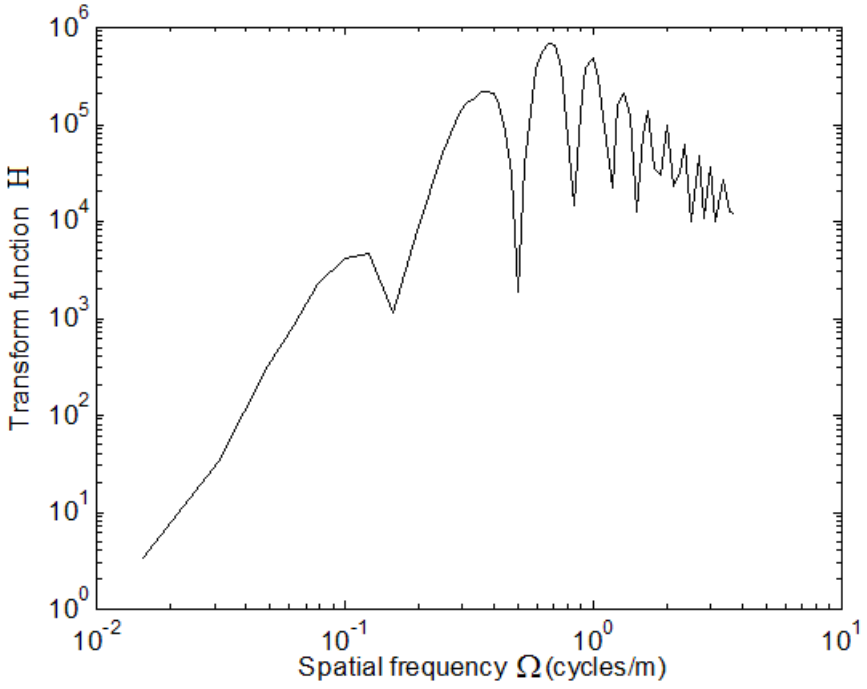

(b)

Figure 7. Transform function ($H(\Omega)$) for: (a) Front and rear axle accelerations, (b) Body accelerations

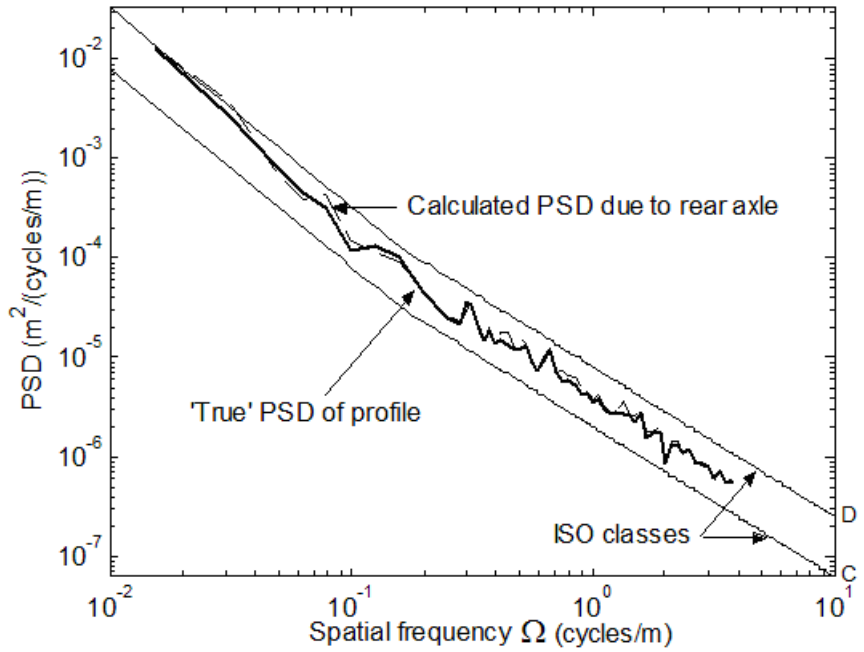

(a)

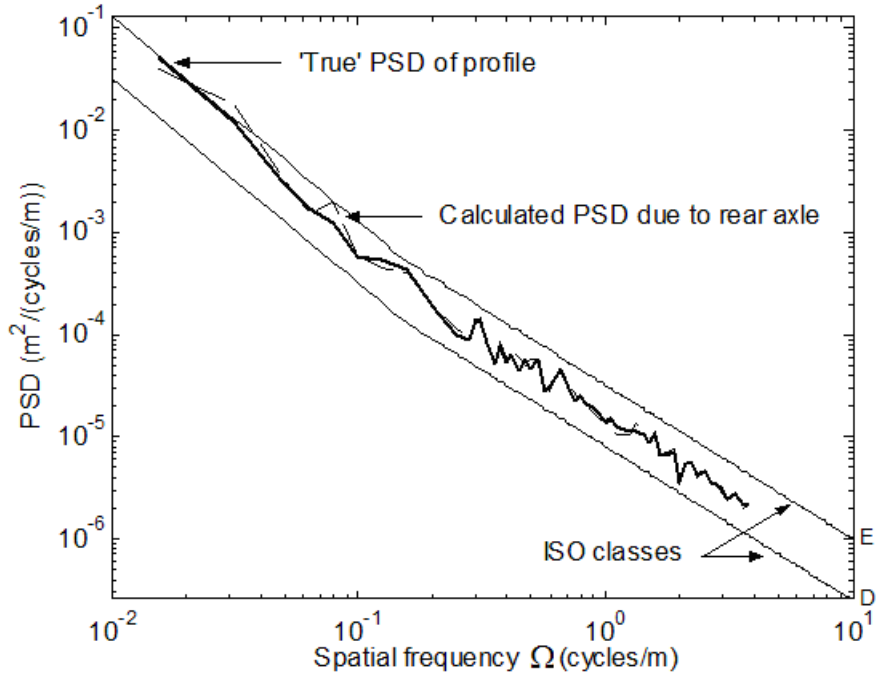

(b)

Figure 8. Comparison of 'true' and estimated *PSD*(Ω) of road profile using front axle accelerations: (a) Class 'C' profile, (b) Class 'D' profile

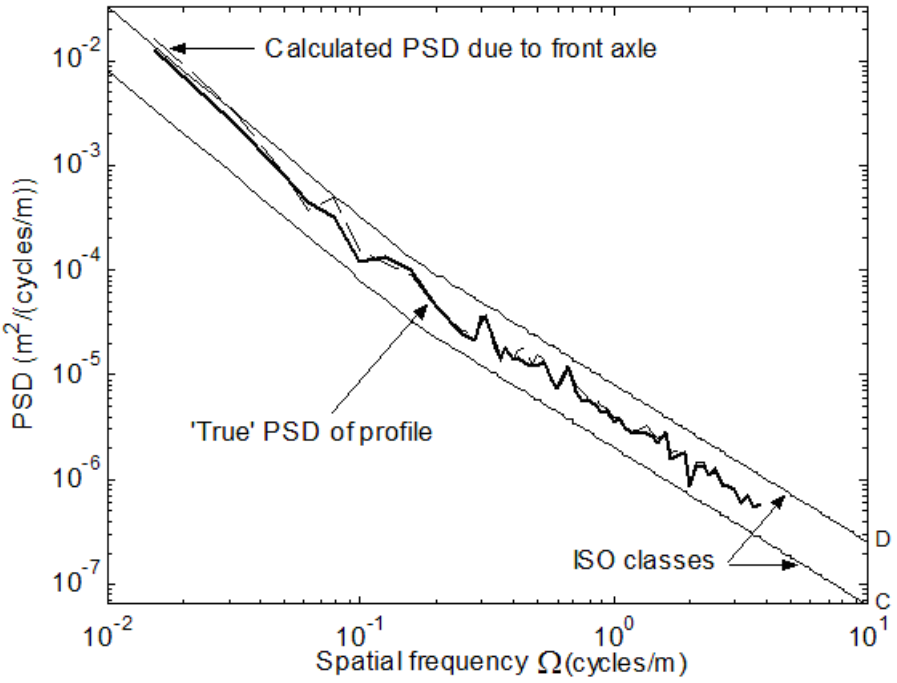

(a)

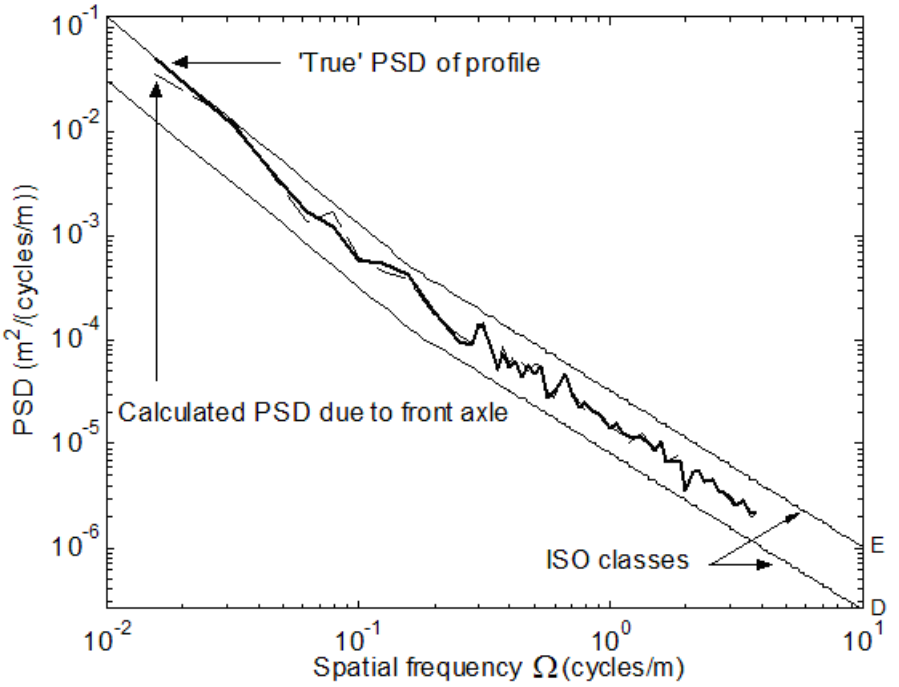

(b)

Figure 9. Comparison of 'true' and estimated *PSD*(Ω) of road profile using rear axle accelerations: (a) Class 'C' profile, (b) Class 'D' profile

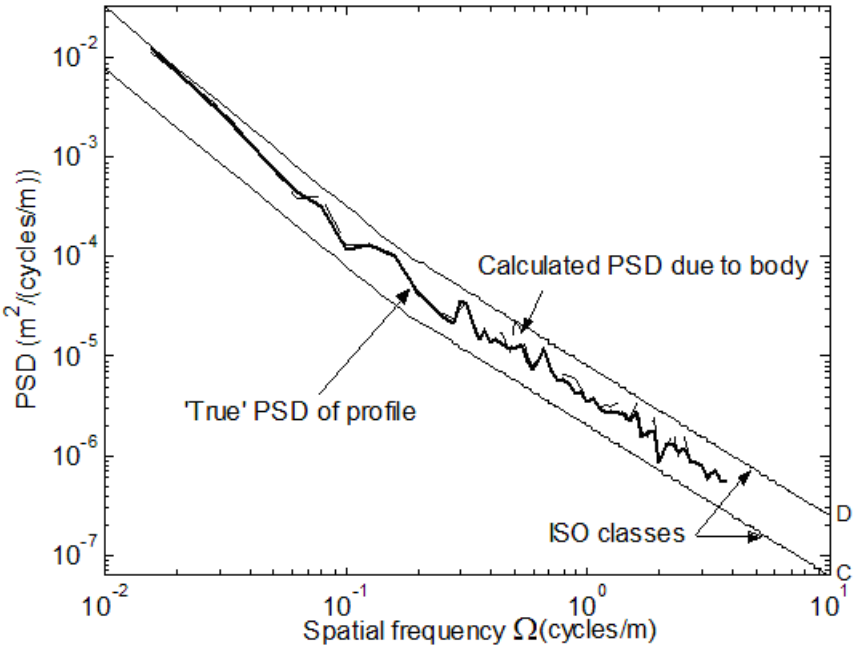

(a)

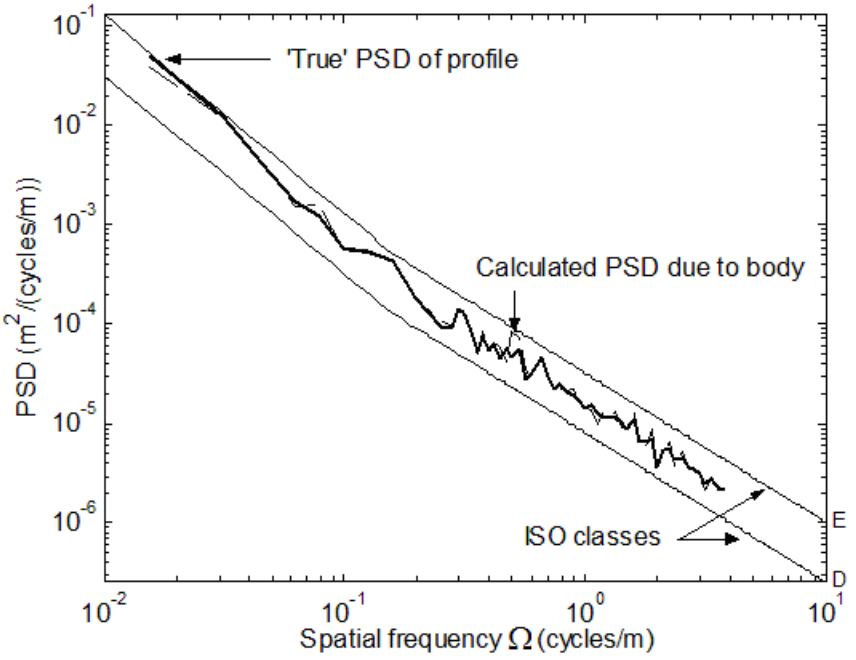

(b)

Figure 10. Comparison of 'true' and estimated *PSD*(Ω) of road profile using body accelerations: (a) Class 'C' profile, (b) Class 'D' profile

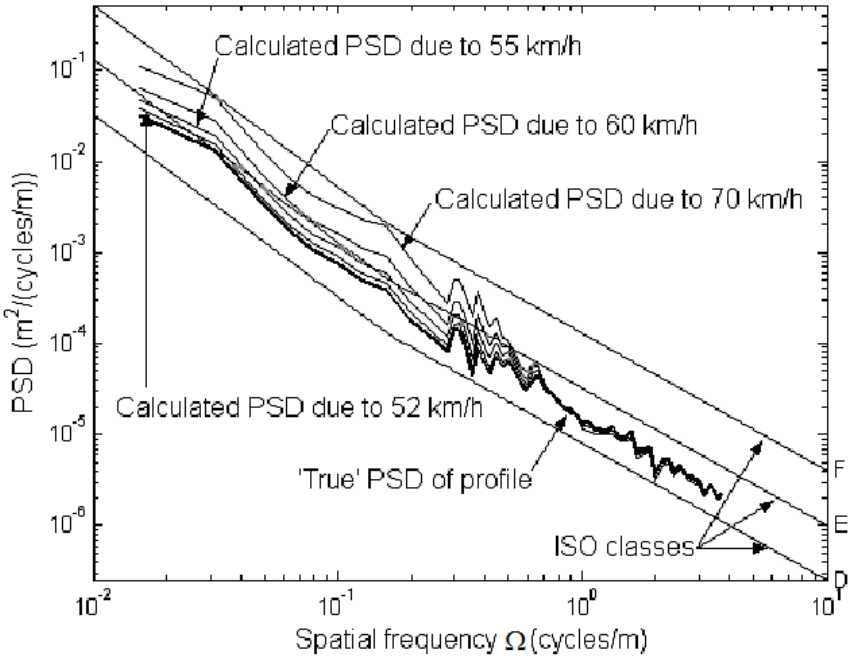

Figure 11. Comparison of 'true' and estimated *PSD*(Ω) of profiles for a range of speeds

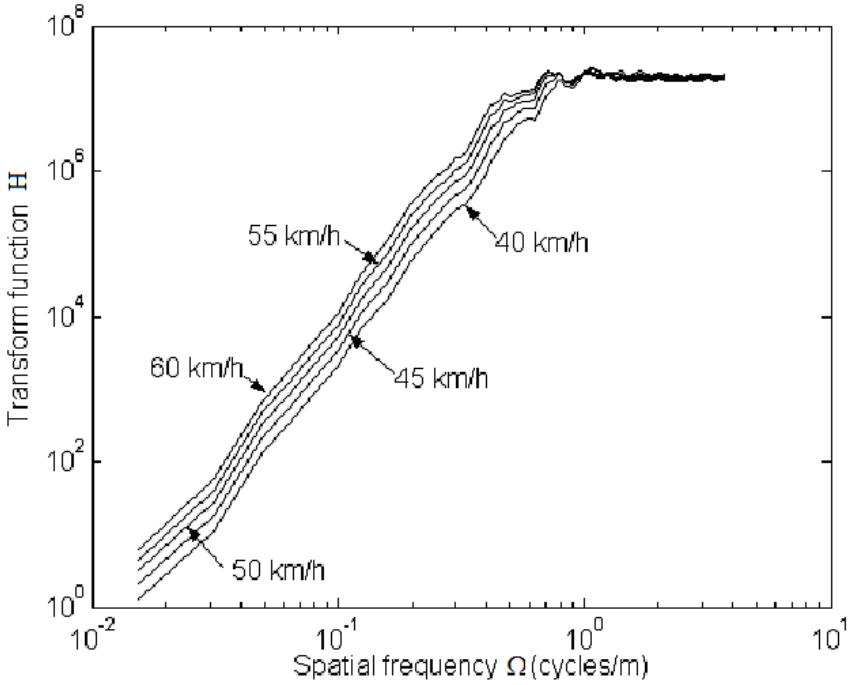

Figure 12. Transform function ($H(\Omega)$) for a range of speeds

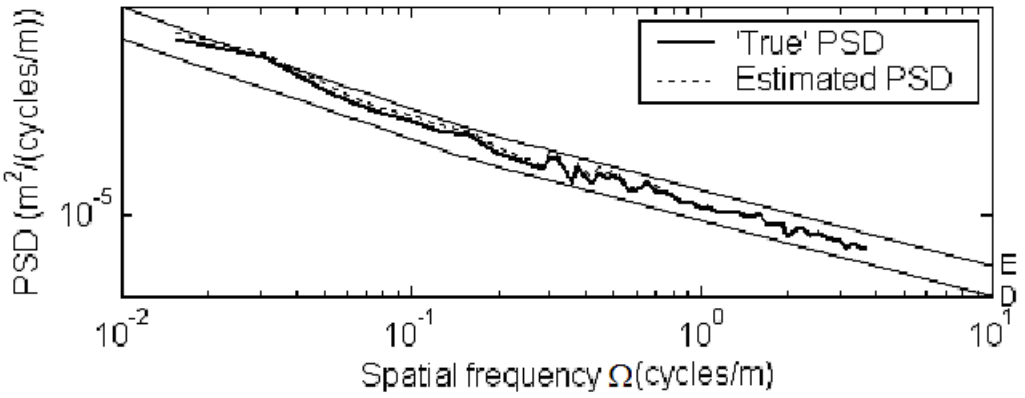

Figure 13. Comparison of 'true' and estimated *PSD*(Ω) of profiles at 42 *km/h*

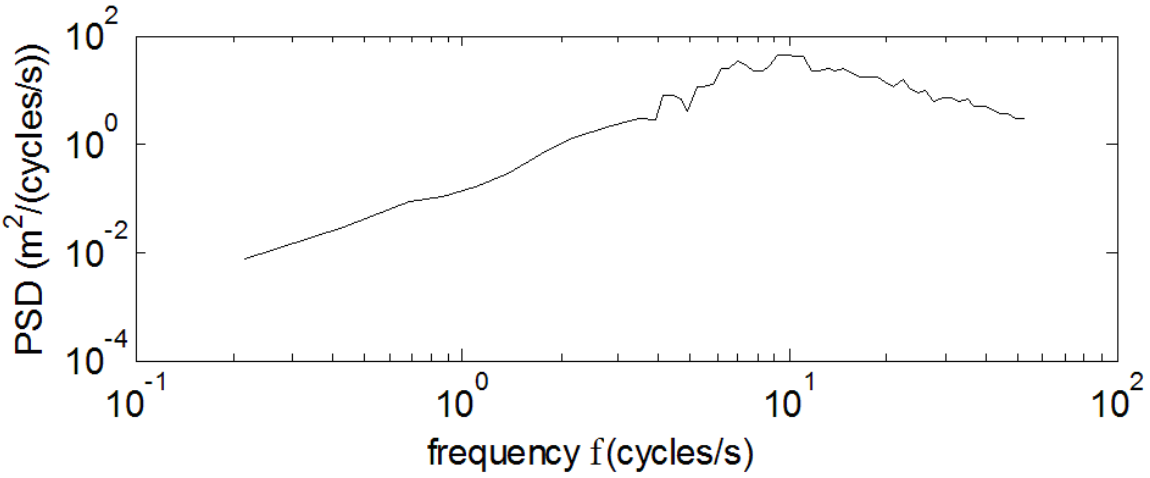

Figure 14. *PSD*(f) of the front axle accelerations versus temporal frequency (f in *cycles/s*)

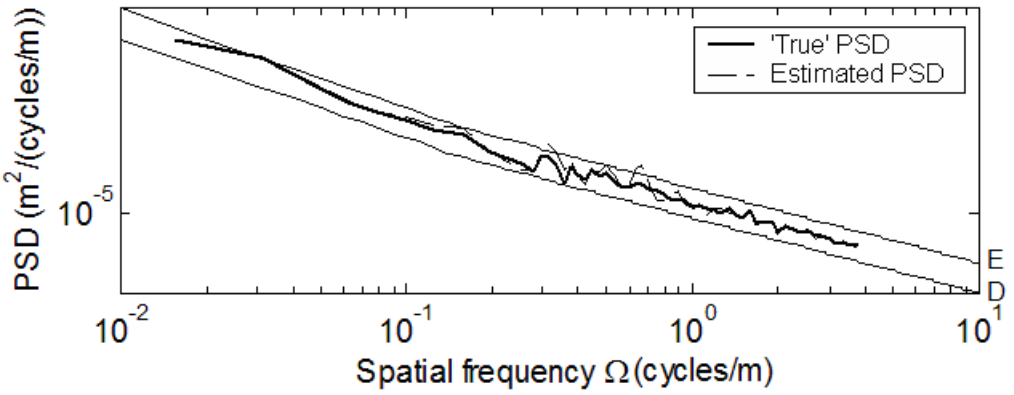
'True' PSD
Estimated PSD
PSD (m²/(cycles/m))
10⁻⁵
10⁻²
10⁻¹
10⁰
10¹
Spatial frequency Ω (cycles/m)
E
D

(a)

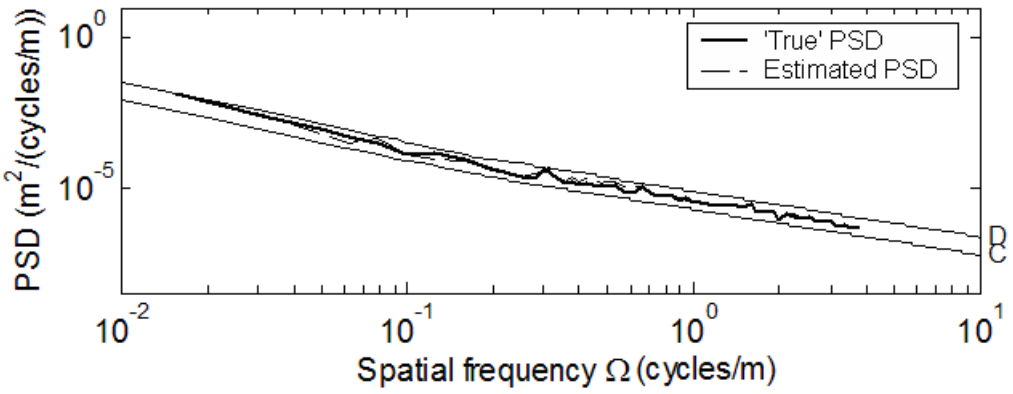
'True' PSD
Estimated PSD
PSD (m²/(cycles/m))
10⁰
10⁻⁵
10⁻²
10⁻¹
10⁰
10¹
Spatial frequency Ω (cycles/m)
D
C

(b)

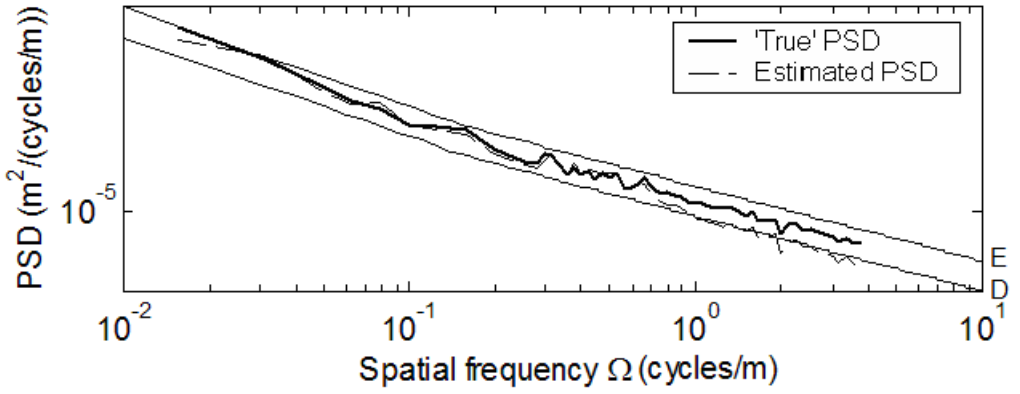
'True' PSD
Estimated PSD
PSD (m²/(cycles/m))
10⁻⁵
10⁻²
10⁻¹
10⁰
10¹
Spatial frequency Ω (cycles/m)
E
D

(c)

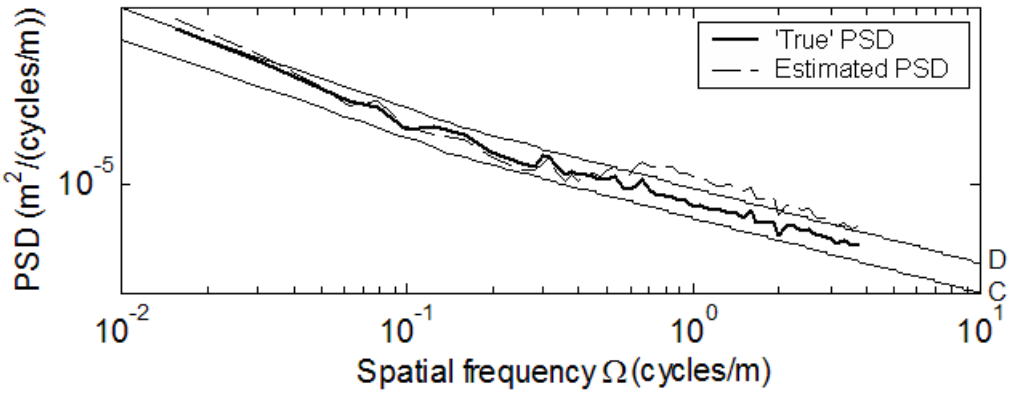

(d)

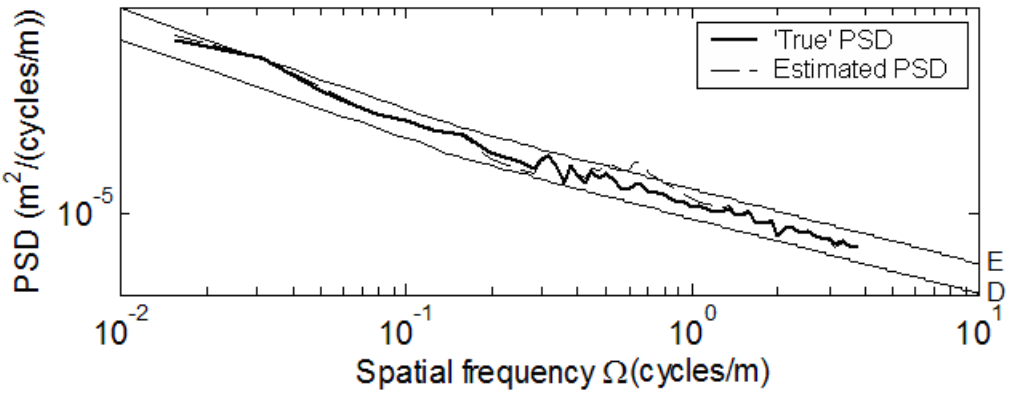

(e)

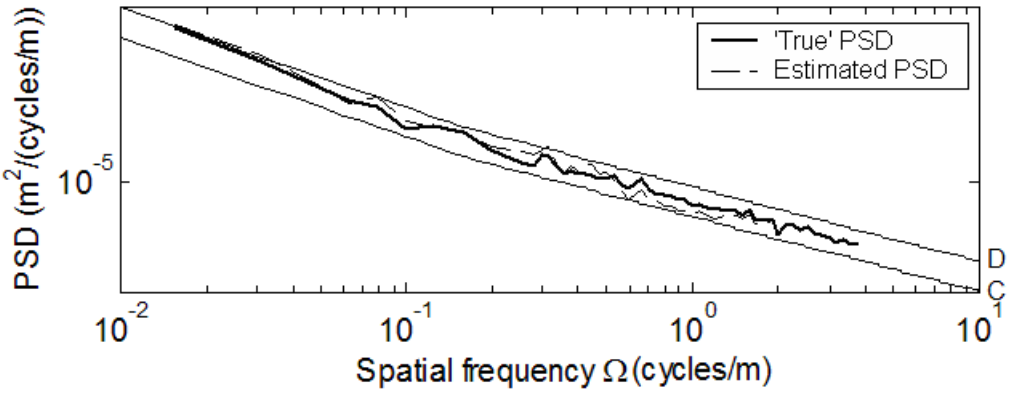

(f)

Figure 15. Comparison of 'true' and estimated *PSD*(Ω) of profiles for a range of vehicle parameters

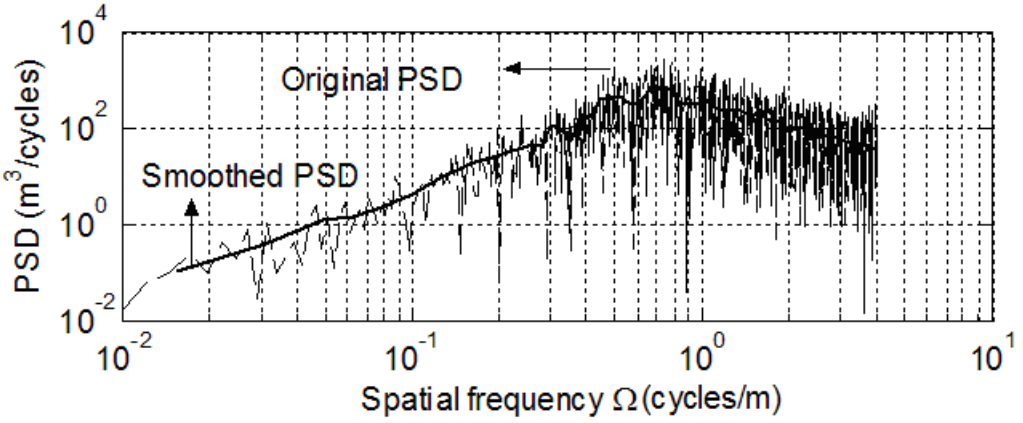
Original PSD
Smoothed PSD
PSD (m3/cycles)
Spatial frequency Ω (cycles/m)

(a)

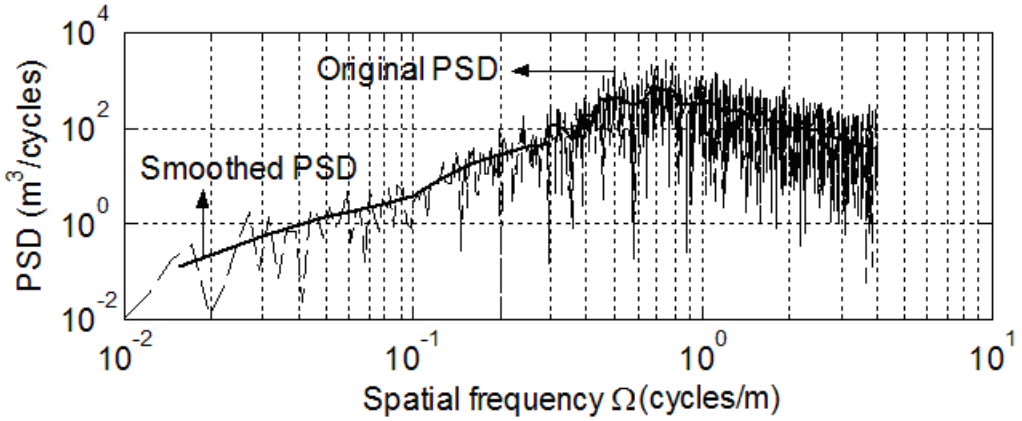
Original PSD
Smoothed PSD
PSD (m3/cycles)
Spatial frequency Ω (cycles/m)

(b)

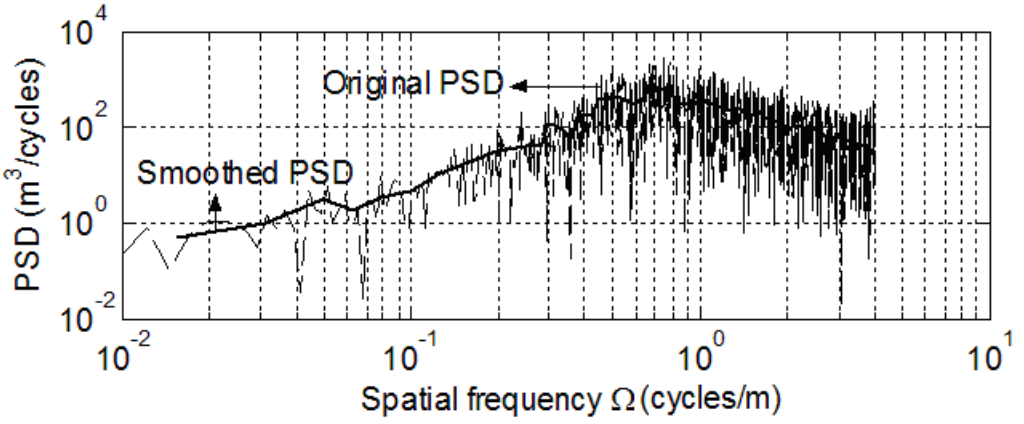
Original PSD
Smoothed PSD
PSD (m3/cycles)
Spatial frequency Ω (cycles/m)

(c)

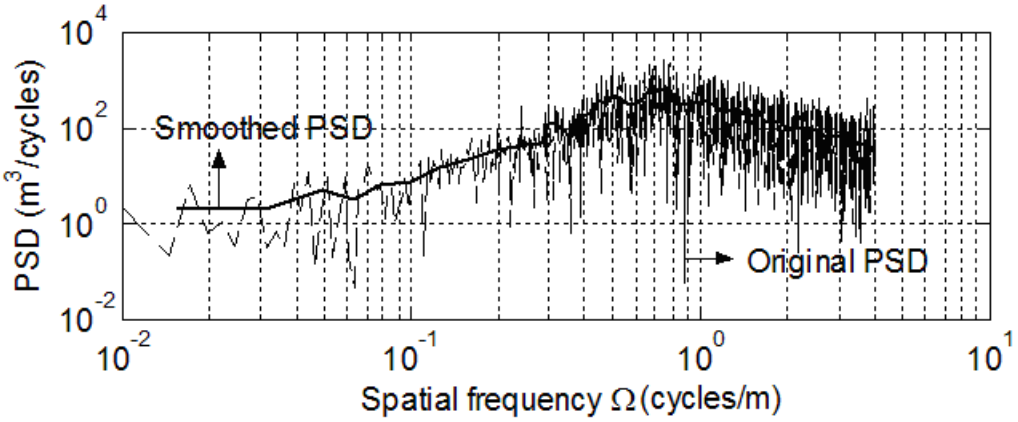

(d)

Figure 16. Original and Smoothed *PSD*(Ω) of front axle accelerations for noise levels of : (a) noise-free, (b) S/N=20, (c) S/N=10 and (d) S/N=5

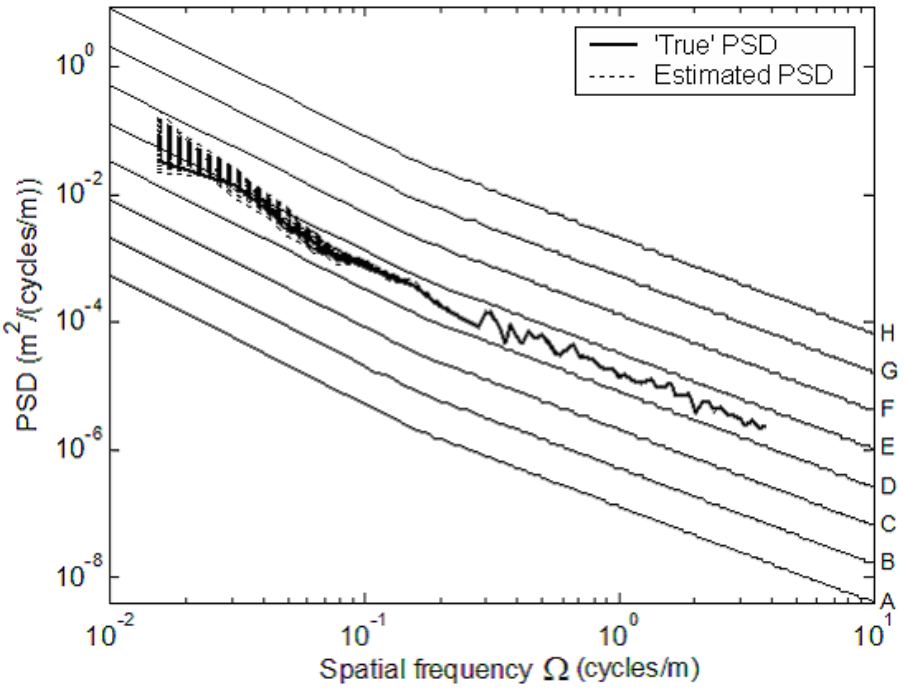
'True' PSD
Estimated PSD
PSD (m²/(cycles/m))
Spatial frequency Ω (cycles/m)
H
G
F
E
D
C
B
A

(a)

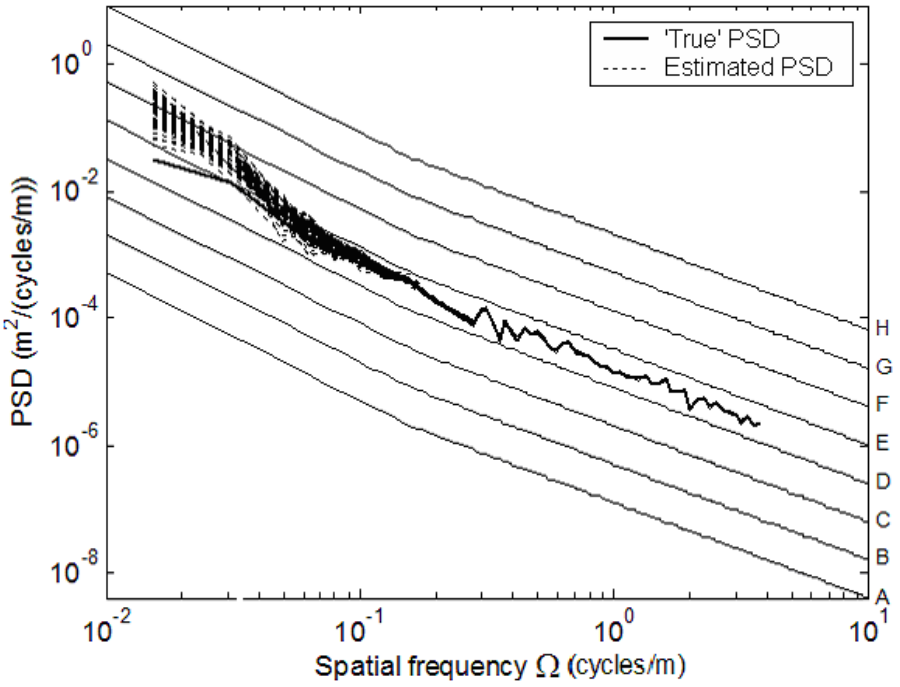
'True' PSD
Estimated PSD
PSD (m²/(cycles/m))
Spatial frequency Ω (cycles/m)
H
G
F
E
D
C
B
A

(b)

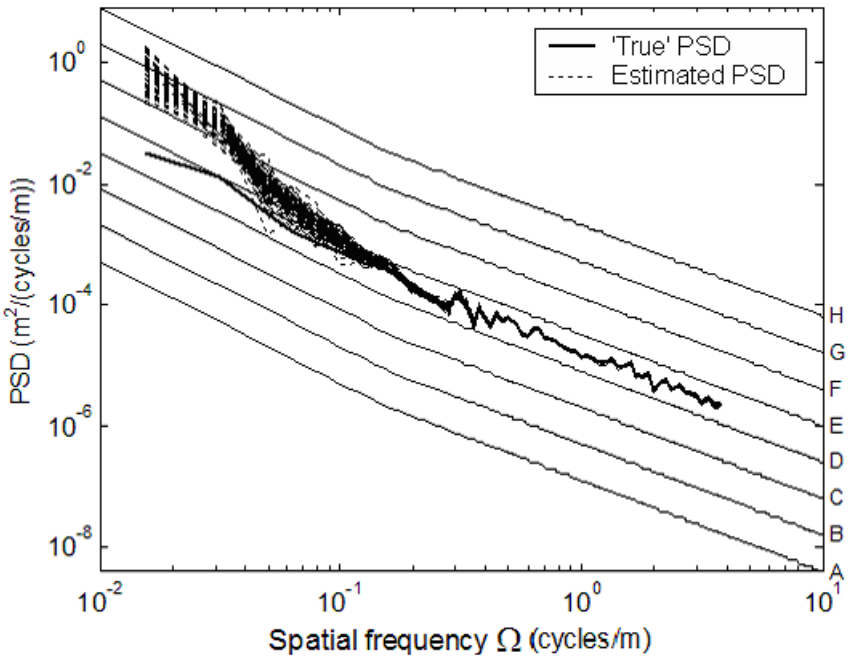

(c)

Figure 17. Comparison of 'true' and estimated *PSD*s(Ω) of road profile from 100 randomly generated noise-corrupted axle accelerations with: (a) *S*/*N*=20, (b) *S*/*N*=10 and (c) *S*/*N*=5

List of tables

Table 1. Parameters of 'typical' half-car model

Spacings (m)		masses (kg)				Stiffness (kN/m)		
D_1	D_2	m_1	m_2	m_3	I_3 (kg/m^2)	K_t	K_s	C_s(kNs/m)
1.5	1.5	181	181	1814	1965	704	88	10.884

Table 2. Parameters of test vehicles

Symbols	Case 1	Case 2	Case 3	Case 4	Case 5	Case 6
D_1 (m)	2.5	2.0	1.5	1.5	1.5	1.5
D_2 (m)	2.5	1.0	1.5	1.5	1.5	1.5
m_1(kg)	181	181	271.5	181	271.5	181
m_2(kg)	181	181	271.5	181	271.5	181
m_3(kg)	1814	1814	2721	1814	2721	1814
I_3 (kg/m^2)	4384	1965	2948	1965	2948	1965
K_t (kN/m)	704	704	704	1056	1056	704
K_s (kN/m)	88	88	88	132	132	88
C_s (kNs/m)	10.884	10.884	10.884	10.884	10.884	15
c (km/h)	41	48	54	59	60	51
Front axle hop (Hz)	10.56	10.56	8.62	12.93	10.55	10.56
Body bounce (Hz)	2.12	2.31	1.73	2.6	2.12	2.12
Body pitch (Hz)	1.48	1.32	1.2	1.81	1.48	1.48
Road class	D	C	D	C	D	C